J|A|C|S COMMUNICATIONS

Published on Web 06/22/2009

Quaternary Alloy Semiconductor Nanobelts with Bandgap Spanning the Entire Visible Spectrum

Anlian Pan,† Ruibin Liu, Minghua Sun, and Cun-Zheng Ning*

Department of Electrical, Computer and Energy Engineering, Arizona State University, Tempe, Arizona 85287

Received May 21, 2009; E-mail: cning@asu.edu

The ability to engineer and control compositions of semiconductor alloys is one of the ultimate goals of semiconductor material science and engineering. Nanomaterials such as nanowires and nanobelts offer an unprecedented opportunity for alloy composition control in a wide range, unavailable with traditional epitaxial film materials, and have attracted a great deal of attention recently, with special focus on achieving a wide range of bandgaps through various ternary alloys.[1−8] For their greater flexibility in composition control and bandgap modulation, quaternary alloy semiconductors can have wider potential applications in tunable optoelectronic devices than the ternary alloys.[9−11] Despite having such great advantages, quaternary alloy semiconductor nanowires or nanobelts have never been achieved to the best of our knowledge, while quaternary alloy thin films are very often achieved in a very limited composition range due to lattice mismatch between alloy materials and the substrate. Here we demonstrate for the first time the growth of quaternary semiconductor alloy nanostructures using an example of $Zn_xCd_{1-x}S_ySe_{1-y}$ ($0 \le x, y \le 1$) nanobelts. We also achieved a controllable variation of the alloy compositions, leading to a tunable bandgap change in the entire visible spectrum. Such unique nanostructured materials with controllable alloy composition will open a wide range of applications in color engineered display and lighting, multispectral detectors, full-spectrum solar cells, and superbroadly tunable nanolasers.

The quaternary ZnCdSSe nanobelts were synthesized through an improved cothermal evaporation route in the presence of Au as a catalyst. A $^1/_4$"-diameter quartz minitube was placed horizontally inside a 1"-diameter quartz tube for transporting the reaction reagent vapors in a confined space to the downstream reaction zone. Before growth, some amount of commercial-grade ZnS and CdSe (Alfa Aesar, 99.995% purity) were loaded independently at two different locations inside the minitube. ZnS powder was positioned at the center of the furnace, while CdSe powder was placed upstream and 12.5 cm from the center of the furnace. A piece of quartz sheet presputtered with 5 nm of Au film was positioned downstream of the system, ~14 cm away from the center of the furnace. The tube reactor was evacuated and back-flushed with Ar/H_2-5% gas until the desired pressure of 50 Torr was reached. A constant flow of 50 sccm was used during the growth. The temperature at the furnace center was set to 1050 °C with a heating rate of 40 °C/min and maintained at its peak temperature for 30 min. The temperature of the locations where ZnS and CdSe powder loaded is 1050 and 970 °C, respectively. Quaternary alloy nanobelts with different compositions can be achieved by changing the relative molar ratio of ZnS and CdSe in the source materials. The experimental setup and growth conditions are schematically shown in Figure S1 (see the Supporting Information (SI)).

† On leave from Key Laboratory for Micro-Nano Optoelectronic Devices of Ministry of Education, and Micro-Nanotechnology Research Center, Hunan University, Changsha, 410082, China.

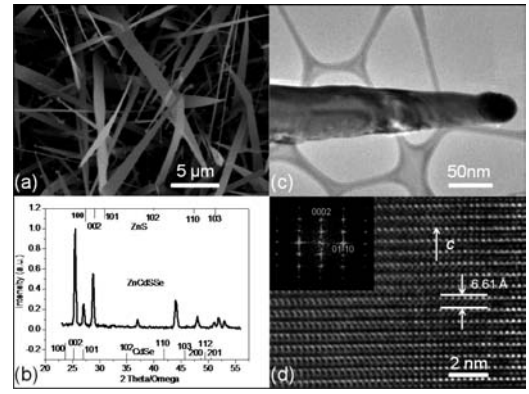

Figure 1. (a) Typical SEM morphology of the obtained quaternary $Zn_xCd_{1-x}S_ySe_{1-y}$ nanobelts; (b) XRD pattern of a representative nanobelt sample; (c and d) TEM image of a single quaternary nanobelt and its corresponding HRTEM image and FFT pattern (inset).

Figure 1a shows the representative scanning electron microscopy (SEM) images of the as-prepared quaternary semiconductor samples. The SEM result indicates that all the samples with different alloy compositions have a similar belt-like morphology, with a typical length of 20−60 μm and width of 1−2 μm. All the belts taper at the growing end with the size down below 50 nm at the tip. The SEM-equipped energy-dispersive X-ray spectroscopy (EDX) analysis demonstrates that all the as-grown nanobelt samples are composed of elements Zn, Cd, S, and Se. X-ray diffraction (XRD) analysis indicates that all the as-grown samples have a pure hexagonal crystallographic phase, with diffraction peaks in between those of hexagonal ZnS and CdSe single crystals (see Figure 1b for the XRD pattern of a representative sample and the standard 2θ values for wurtzite ZnS and CdSe single crystals). Transmission electron microscopy (TEM) was used to further investigate the microstructures of single quaternary alloy belts. Figure 1c shows the representative TEM image of the achieved quaternary alloy nanobelts, with a catalyst particle at the tip, indicating the metal catalyzed Vapor−Liquid−Solid growth of the belts. The high-resolution TEM (HRTEM) observations (Figure 1d) as well as its corresponding fast Fourier transform (FFT) analysis (see the inset) demonstrate that the obtained nanobelts have single-crystal and wurtzite hexagonal structure, which is consistent with the XRD measurements (Figure 1b). The measured (0001) interplanar spacing (c value) is also in good agreement with that deduced from the XRD patterns. All these macro- and microstructural characterizations support the formation of quaternary ZnCdSSe nanostructured alloys.

Scanning transmission electron microscopy X-ray energy dispersive spectrometry (STEM-XEDS) was utilized to further investigate the nanoscale elemental composition as well as the spatial uniformity of element distribution in the quaternary alloy belts. Figure 2a is a TEM image of an examined belt for composition

10.1021/ja904137m CCC: $40.75

measurement, and Figure 2b shows the corresponding EDX data collected from a single point in the belt, confirming the existence of elements Zn, Cd, S, and Se in single nanobelts (with element Cu coming from the copper grid hold). Figure 2c−f show, respectively, two-dimensional (2D) elemental mapping of this belt for the four elements without any apparent element separation or aggregation exhibited, demonstrating that all the four elements, Zn, Cd, S, and Se, are very homogeneously distributed across the belts. The EDX analysis from several selected points along the length of a single belt indicates that the composition is also uniform along the full length of the nanobelts.

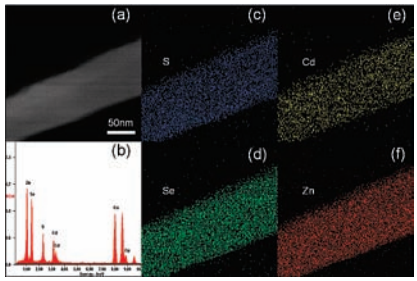

Figure 2. (a)TEM image of an examined quaternary belt and its corresponding EDX profile measured from a point in the belt; (c−f) 2D element mapping for the detected four elements, Zn, Cd, S, and Se, respectively.

The composition of alloy nanobelts is usually determined by the relative ratio of source materials and the deposition temperature on the substrate. For a short substrate, the substrate temperature depends on its location along the tube axis. Thus alloy composition can be controlled by the source materials ratio, by substrate location, or a combination of the two. At a fixed location, the alloy compositions of the belts can be easily varied through changing the molar ratio of the two source powders (ZnS/CdSe). Table S1 (see the SI) gives the composition (x and y) information deducted from EDX analysis of several representative $Zn_xCd_{1-x}S_ySe_{1-y}$ ($0 \leq x, y \leq 1$) alloy nanobelt samples, and Figure 3 presents their corresponding normalized photoluminescence (PL) spectra, using a pulsed frequency-quadrupled Nd:YAG laser (266 nm) as the pump source. The spectra of all samples show a single emission band, with the peak wavelength continuously shifted from 361 to 712 nm covering the entire visible region. The standard interpolation formula for quaternary semiconductor alloys $A_xB_{1-x}C_yD_{1-y}$[12] was used to obtain the band gap of $Zn_xCd_{1-x}S_ySe_{1-y}$ alloys as functions of composition variables x and y.[9] The PL peak values for each of the nanobelt samples and the corresponding interpolated band gap values are also shown in Table S1 (see the SI). The high degree of consistence between the spectral measurements and the interpolations demonstrates that the peak position tunable PL of the quaternary nanobelts comes from the composition related band edge emission of the alloy semiconductors. At the same time, the continuous shift of the PL bands for the obtained alloy belts with their compositions gives further evidence for the formation of uniform quaternary $Zn_xCd_{1-x}S_ySe_{1-y}$ alloys via intermixing the wide band gap of ZnS and the narrow band gap of CdSe, rather than the formation of the independent binary or ternary phases, in good agreement with the results of nanoscale 2D elemental mapping (see Figure 2). In addition, all of the quaternary belt exhibits a single band edge emission, without any defect or structural disorder-related low-energy emission detected, further demonstrating that the obtained nanostructures are highly crystallized with few defects, which is also consistent with the HRTEM observations.

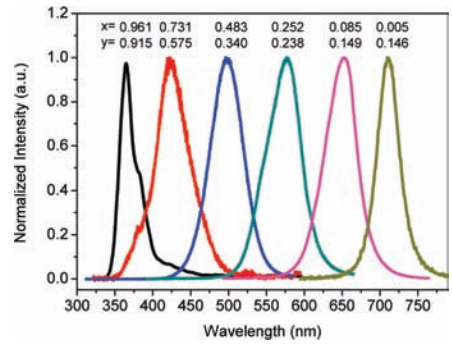

Figure 3. Normalized PL spectra of the achieved quaternary $Zn_xCd_{1-x}S_ySe_{1-y}$ nanobelts excited with a pulsed frequency-quadrupled Nd:YAG laser (266 nm). The data above the spectra show the relative composition x and y values.

In summary, we used an improved cothermal evaporation route to achieve for the first time quaternary alloy semiconductor nanostructures, using $Zn_xCd_{1-x}S_ySe_{1-y}$ nanobelts as an example. The composition of the achieved alloys can be tuned by controlling the molar ratio of the source materials, resulting in their band edge light emission to be continuously tunable across the entire visible spectrum. This material system in its complete band gap range has never been achieved in any form of single crystals, bulk, or nanomaterials. Such widely controlled alloy nanostructures via composition provide a new material platform for a wide range of applications from wavelength-tunable lasers, multicolor detectors, full-spectrum solar cells, LEDs, to color displays, all of which are under active pursuit currently.

Acknowledgment. We thank the US Army Research Office for financial support.

Supporting Information Available: Schematical setup (Figure S1) for the sample growth and its related discussions; Composition and bandgaps of the samples (Table S1). This material is available free of charge via the Internet at http://pubs.acs.org.

References

(1) Kyukendall, T.; Ulrich, P.; Aloni, S.; Yang, P. *Nat. Mater.* **2007**, *6*, 951.
(2) Liu, Y.; Zapien, J. A.; Shan, Y. Y.; Geng, C. Y.; Lee, C. S.; Lee, S. T. *Adv. Mater.* **2005**, *17*, 1372.
(3) Pan, A. L.; Yang, H.; Liu, R.; Yu, R.; Zou, B.; Wang, Z. L. *J. Am. Chem. Soc.* **2005**, *127*, 15692.
(4) Pan, A. L.; Zhou, W.; Leong, E. S. P.; Liu, R.; Chin, A. H.; Zou, B.; Ning, C. Z. *Nano Lett.* **2009**, *9*, 784.
(5) Pan, A.; Yao, L.; Qin, Y.; Yang, Y.; Kim, D. S.; Yu, R.; Zou, B.; Werner, P.; Zacharias, M.; Gosele, U. *Nano Lett.* **2008**, *8*, 3413.
(6) Lim, S. K.; Tambe, M. J.; Brewster, M. M.; Gradecak, S. *Nano Lett.* **2008**, *8*, 1386.
(7) Su, J.; Gherasimova, M.; Cui, G.; Tsukamoto, H.; Han, J.; Onuma, T.; Kurimoto, M.; Chichibu, S. F.; Broadbridge, C. *Appl. Phys. Lett.* **2005**, *87*, 183108.
(8) Liu, Y. K.; Zapien, J. A.; Shan, Y. Y.; Tang, H.; Lee, C. S.; Lee, S. T. *Nanotechnology* **2007**, *18*, 365606.
(9) Feng, Y. P.; Teo, K. L.; Lim, F.; Poon, H. C.; Ong, C. K.; Xia, J. B. *J. Appl. Phys.* **1993**, *74*, 3948.
(10) Vijayalakshmi, R. P.; Venugopal, R.; Reddy, D. R.; Reddy, B. K. *Semicond. Sci. Technol.* **1994**, *9*, 1062.
(11) Marques, M. *Phys. Rev. B* **2006**, *73*, 232205.
(12) Tamargo, M. C. *II-VI semiconductor materials and their applications*; Taylor & Francis: New York, 2002.

JA904137M